Nano Energy 105 (2023) 107980

Contents lists available at ScienceDirect

Nano Energy

journal homepage: www.elsevier.com/locate/nanoen

Promoting industrial-level CO_2 electroreduction kinetics via accelerating proton feeding on a metal-free aerogel electrocatalyst

Wanzhen Zheng [a,1], Dashuai Wang [b,1], Yikai Zhang [a], Sixing Zheng [a], Bin Yang [a,b], Zhongjian Li [a,b], Raul D. Rodriguez [f], Tao Zhang [d], Lecheng Lei [a,b], Siyu Yao [a], Yang Hou [a,b,c,e,*]

[a] Key Laboratory of Biomass Chemical Engineering of Ministry of Education, College of Chemical and Biological Engineering, Zhejiang University, Hangzhou 310027, China
[b] Institute of Zhejiang University - Quzhou, Quzhou 324000, China
[c] Donghai Laboratory, Zhoushan, China
[d] Ningbo Institute of Materials Technology & Engineering, University of Chinese Academy of Sciences, Ningbo 315200, China
[e] School of Biological and Chemical Engineering, NingboTech University, 1 South Qianhu Road, Ningbo, Zhejiang 315100, China
[f] Tomsk Polytechnic University, 30 Lenin Ave, Tomsk 634050, Russia

ARTICLE INFO

Keywords:
Metal-free carbon aerogels
N/P doping
Accelerating proton feeding
CO_2 electroreduction
Zn-CO_2 battery

ABSTRACT

Developing cost-effective carbon based electrocatalysts with high activity and selectivity for CO_2 reduction reaction (CO_2RR) at industrial current density still remains challenges. Herein, we present a metal-free 3D cross-linked carbon aerogel catalyst containing homogeneously dispersed N and P sites (P@NCA) synthesized via freeze drying and subsequent carbonization. Benefit from the synergistic effect of N and P atoms, P@NCA aerogel delivers an excellent CO_2RR activity featured by a wide potential window from − 0.3 V to − 0.9 V with CO Faradaic efficiency (FE) of above 90 %. Importantly, a high CO FE of 85 % at an industrial current density of 100 mA cm^{-2} is realized. Experimental explorations and in-situ spectroelectrochemistry analyses reveal that pyrrolic-N species acts as the real active site to execute CO_2RR, while the P species facilitates the protonation process of *CO_2 to *COOH intermediate by accelerating the proton feeding from water dissociation. Theoretical calculations demonstrate a suppressed *H adsorption and a facilitated *CO desorption step on pyrrolic-N site with P doping, boosting the whole CO_2RR process. Further, a rechargeable Zn-CO_2 battery constructed with P@NCA aerogel as cathode delivers a maximal power density of 0.8 mW cm^{-2} and a superior stability.

1. Introduction

Electrochemical CO_2 reduction reaction (CO_2RR) driven by renewable energy is a promising technology to reduce CO_2 concentration in atmosphere [1,2]. Compared with industrially energy-intensive thermocatalytic reactions, electrocatalytic CO_2RR process can convert CO_2 molecules into high value-added chemicals (CO, ethylene, and formic acid, etc.) under mild conditions [3,4]. In recent years, noble metal and its alloy catalysts, such as Au, Ag, Pd, PdCu, and AgCu, etc., have made good progress in the field of CO_2RR [5]. Especially, carbon-supported metal single atom catalysts (M-N-C, M = Ni, Fe, Co, Cu, and Mn, etc.) presented superior catalytic activity for CO_2RR at high current density in the designed electrolyzers [6,7]. However, these mentioned metal-based catalysts still face several inevitable disadvantages, such as low abundance of earth elements, high cost, and complicated synthesis steps, etc., which seriously hinder the practical industrial utilization of CO_2RR [8,9].

In contrast, metal-free carbon based materials, especially the electrocatalysts featured with unique hierarchical interconnected structures [10] that possess the advantages of low cost, resistance to acids and bases, porous structure with various pores, and environmental friendliness, have a good prospect for the practical application of CO_2RR [11–13]. However, previously reported non-metallic carbon based CO_2RR catalysts, in particular, the widely reported N-doped carbon electrocatalysts, face inevitable problems, such as monotonous active site, slow CO_2 reaction kinetics, and strong competitive hydrogen

* Corresponding author at: Key Laboratory of Biomass Chemical Engineering of Ministry of Education, College of Chemical and Biological Engineering, Zhejiang University, Hangzhou 310027, China.
E-mail address: yhou@zju.edu.cn (Y. Hou).
[1] These authors contributed equally.

https://doi.org/10.1016/j.nanoen.2022.107980
Received 18 August 2022; Received in revised form 1 November 2022; Accepted 2 November 2022
Available online 3 November 2022

evolution reactions (HER), thus resulting in low CO_2RR activity [9,14]. Despite the simple synthesis method, N-doped carbon materials still display poor catalytic performance in CO_2RR, which is difficult to achieve industrial current density and wide potential window. Moreover, the carbon catalyst doped only with N element cannot achieve the desired catalytic performance due to the strong *H adsorption on N sites that often causes competitive HER [15,16]. The introduction of additional heteroatoms (P, S, F, and Se, etc.) can efficiently change the electronic structure of N-doped carbon catalysts. Under the synergistic effect of di-heteroatoms (N/S, N/P, N/Se, N/F, etc.), the adsorption strength of key intermediates (*COOH or *CO) of CO_2RR on active site will be enhanced or weakened, thus achieving catalytic performance enhancement [8,17], which has considered as an effective method to boost CO_2RR activity and suppress the HER [11,18]. Compared with other heteroatoms (S, Se, and F), foreign P atom has the largest atomic radius and lowest electronegativity (P < Se < S < F), thus the doping of P atom would possess the highest possibilities of adjusting the electronic structure of N atoms, thereby optimizing the adsorption free energy of key intermediates in CO_2RR. Despite certain progress on CO_2RR catalyzed by di-heteroatoms doped carbon catalysts, the catalytic current density is still low in most cases. Especially, achieving high CO Faradaic efficiency (FE) under industrial current density ($\geq$ 100 mA cm^{-2}) and wide potential window are still challenging in CO_2RR, meanwhile, understanding the reaction mechanism and identifying actual active site of di-heteroatoms in CO_2RR are urgently needed [19,20].

Herein, we report a metal-free carbon aerogel CO_2RR catalyst featuring diatomic N-P sites (P@NCA) which was prepared via a radical polymerization, followed by a high temperature carbonization treatment under ammonia atmosphere. Benefited by the unique 3D interconnected structure with homogeneous meso-pores distribution and highly exposed N, P sites, P@NCA aerogel displays high CO FE of above 90 % at a wide potential window from − 0.3 V to − 0.9 V via CO_2RR. As-prepared P@NCA aerogel also achieves an industrial-level current density of 100 mA cm^{-2} with a CO FE of 85 %, outperforming a majority of other reported metal-free carbon based CO_2RR electrocatalysts. A series of controlled experiments and structural characterizations demonstrate the pyrrolic-N species acted as actual active sites in CO_2RR. In-situ attenuated total reflectance-Fourier transform infrared (ATR-FTIR) confirms under the regulation of surrounding P atoms, the water dissociation step and subsequent CO_2 protonation process (*CO_2-*COOH) on pyrrolic-N site is significantly promoted. Theoretical calculations reveal that the P dopants induce the increase of charge density over the pyrrolic-N site, which enhances the CO desorption from active pyrrolic-N, thereby improving the CO_2-CO selectivity. When assembled as cathode in rechargeable Zn-CO_2 battery, the newly-developed P@NCA aerogel display a high power density of 0.8 mW cm^{-2} and long-term stability of 20 h for CO production.

2. Experimental section

2.1. Synthesis of P@NCA aerogel

2.76 mL of phytic acid (50 wt% in water) and 6 mL of deionized water (DI water) were added into a bottle under vigorous stirring for 5 min. Then, 1.65 mL of aniline solution was added into above bottle and stirring for 10 min. Next, 0.855 g of ammonium persulfate (APS) was dissolved in 3 mL DI water. After cooling to 4 °C, the APS solutions were added into the bottle and keep stirring for 10 min. The fully reacted mixture was transferred into the refrigerator and kept at 4 °C for 12 h to obtain P@NCA hydrogels precursor. Then, the obtained precursor was centrifuged and washed three times with anhydrous ethanol and DI water, respectively, and then freeze-drying for 24 h under vacuum. Finally, the sample was put in a tube furnace and heated to 1000 °C with a rate of 3 °C min^{-1}, then kept for 1 h in 10 % NH_3/N_2 atmosphere. After cooling to room temperature, the P@NCA aerogel was obtained.

2.2. Synthesis of NCA aerogel

The synthesis procedure for NCA aerogel is similar to that of P@NCA aerogel, except adding the phytic acid, the obtained sample was named as NCA aerogel.

2.3. Synthesis of P@CA aerogel

2.76 mL of phytic acid (50 wt% in water) and 6 mL of DI water were added into a bottle under vigorous stirring for 5 min. Next, 200 mg of carbon black with 20 mL of DI water was added into above bottle and keeps stirring for 2 h. Then, the formed mixture was placed in a centrifuge tube and freeze-dried for 24 h. Finally, the obtained sample underwent a same carbonization process with P@NCA, the sample of P@CA aerogel was obtained.

2.4. Electrochemical measurements

The performance of electrochemical CO_2 reduction over as-prepared catalysts was performed in flow cell and H-cell equipped with three-electrode system on the electrochemical work station (CHI 760E). The electrolyte in H-cell and flow cell was CO_2-saturated 0.5 M $KHCO_3$ and 1.0 M $KHCO_3$ solution, respectively. Both the anodic and cathodic electrolyte chambers in H-cell and flow cell were separated by the cation exchange membrane (Nafion 117, DuPont). In H-cell, the highly purified CO_2 gas (99.999 %) was injected into the cathodic electrolyte with a flow rate of 20 mL min^{-1}, while in flow cell, the CO_2 (99.999 %, 20 mL min^{-1}) was injected into the chamber in the backside of working electrode. The reference electrodes used in H-cell and flow cell were Ag/AgCl electrode; and the counter electrode was Pt wire and Ni foam in H-cell and flow cell, respectively; the details of working electrode preparation can be found in Supporting Information. The linear sweep voltammetry curve was performed under the range of 0 to − 1.2 V with the scan rate of 5 mV s^{-1}, the electrochemical impedance spectrum was tested under 10 mV AC voltage, along with the frequency range from 10 mHz to 10 KHz.

2.5. DFT analysis

The theoretical calculations were performed by using Vienna ab initio simulation package. A plane wave cutoff energy of 400 eV was used. The generalized gradient approximation proposed by Perdew, Burke, and Ernzerhof was utilized in the projector-augmented wave method. Additional details can be found in Supporting Information.

3. Results and discussion

The 3D catalyst of metal free P@NCA aerogel was synthesized through a low temperature polymerization and high temperature carbonization method (Fig. S1), in which phytic acid and aniline monomer were selected as P and N sources, respectively [21]. When mixed two reactants, a protonating reaction of the N groups in aniline happened to generate phytic acid-aniline composite. After the oxidative initiator of ammonium persulfate added, corresponding polyaniline-phytic acid hydrogel was formed under the ionic-polymerization reaction (Figs. S2–S4) [22,23]. Followed by freeze drying and carbonization at 1000 °C in ammonia atmosphere, the P@NCA hydrogel was convert to produce the final product of P@NCA aerogel (Figs. S5–S6). During the carbonized process, the N and P atoms are gradually activated with the increase of temperature, and the evaporation of carbon leads to large surface area and highly exposed active sites, which can effectively enhance the performance of electrochemical CO_2RR [24].

Transmission electron microscopy (TEM) image of P@NCA aerogel (Fig. 1a) showed a unique 3D cross-linked characteristic with particle size of about 100 nm [25]. Further high-resolution TEM (HRTEM) image

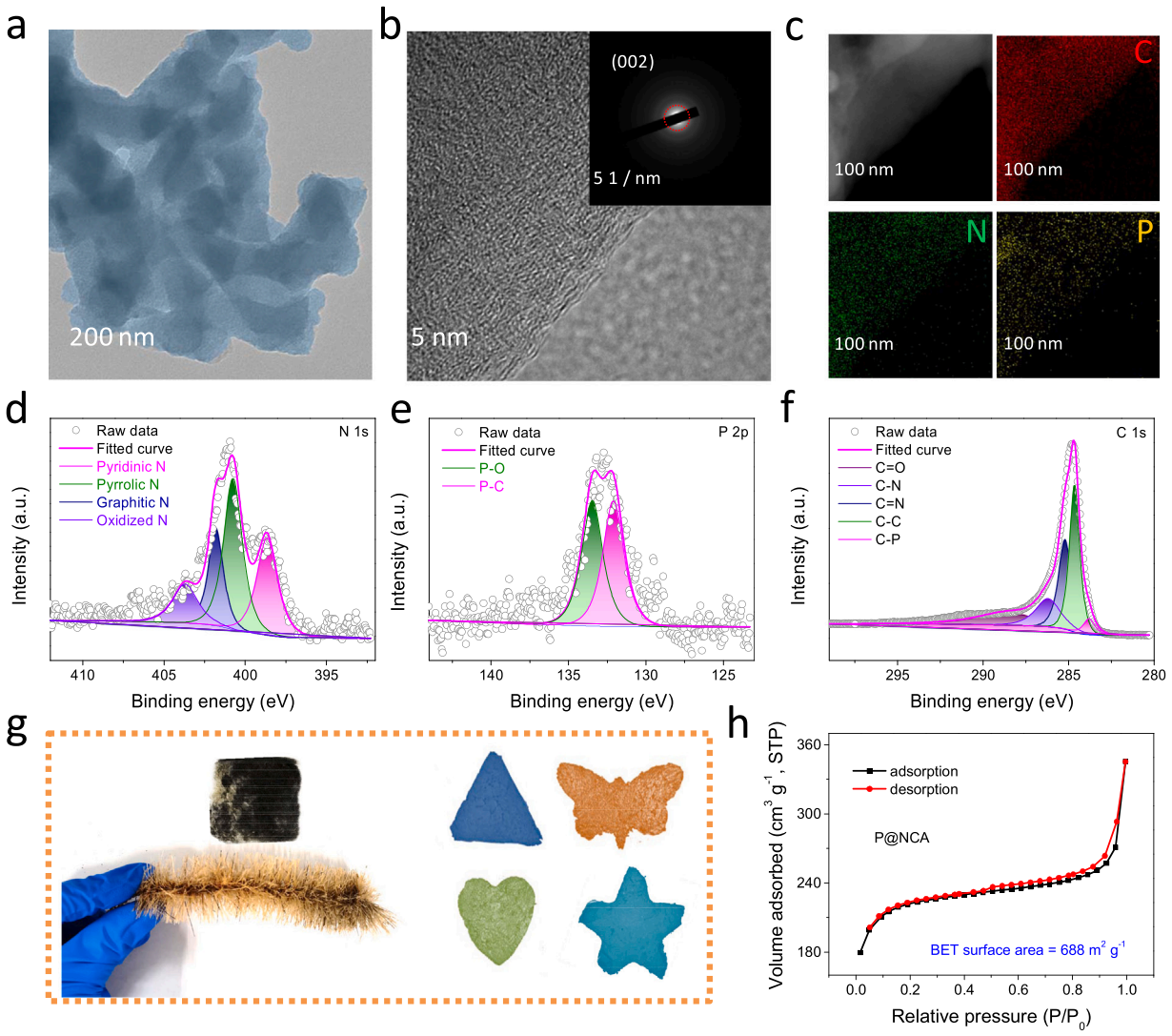

Fig. 1. (a-b) TEM and HRTEM images of P@NCA (inset: SAED pattern), (c) EDX elemental mappings of C, N, and P for P@NCA, (d–f) high resolution N 1s, P 2p, and C 1s XPS spectra of P@NCA, (g) digital photo of metal-free carbon aerogel prepared and its different shapes, (h) N_2 adsorption-desorption isotherm curve of P@NCA.

of P@NCA aerogel displayed a lattice fringe distance of 0.34 nm in edge (Fig. 1b and Fig. S7), which is attributed to (002) plane of graphitized carbon [26,27]. The corresponding inset image of selected area electron diffraction (SAED) pattern exhibited a typical ring belong to the (002) plane of carbon, which is well supported by X-ray diffraction (XRD) results (Fig. S8) [28,29]. Energy-dispersive X-ray spectroscopy (EDX) showed a homogeneous distribution of C, N, and P elements in the P@NCA aerogel (Fig. 1c) [30]. X-ray photoelectron spectroscopy (XPS) spectra of P@NCA aerogel further confirmed the co-existence of C, N, O, and P elements (Figs. S9–S12). For the high-resolution N 1s XPS spectrum of P@NCA aerogel, four different types of N species were identified as pyridinic-N (398.6 eV), pyrrolic-N (400.7 eV), graphitic-N (401.8 eV), and oxidized-N (403.7 eV), respectively (Fig. 1d) [31]. The high-resolution P 2p XPS spectrum of P@NCA aerogel (Fig. 1e) showed two typical chemical bonds of P-C and P-O located at 132.1 eV and 133.4 eV, respectively [32]. The C-N bond (286.3 eV) and C-P bond (283.8 eV) were also observed in P@NCA aerogel as detected by high-resolution C 1s XPS spectrum (Fig. 1f). Both of them proved the existences of C-N and C-P bonds, suggesting the successful synthesis of P@NCA aerogel. Notably, the shapes of P@NCA aerogel can be molded into various models (Fig. 1g), for example, the cylindrical P@NCA model stranded on yellow flower, indicating the lightness of this aerogel, other prepared models of triangle, butterfly, heart, and pentagram, indicating the processability of as-prepared aerogel [33]. Raman spectra of P@NCA aerogel showed an increased intensity ratio of D and G bands compared with other mono-doped samples, indicating the riched defects structure (Fig. S13) [34,35]. The Brunauer-Emmett-Teller (BET) surface area of P@NCA aerogel was determined to be 688 m^2 g^{-1} with an average pore size of 6 nm (Fig. 1h and Fig. S14), demonstrating the mesoporous structure of P@NCA aerogel, in favor of CO_2 transfer and adsorption [36].

The CO_2RR performances of P@NCA aerogel were tested in a flow-cell reactor to eliminate the mass transfer effects of CO_2, in which gas diffusion layer (GDL) loading the catalyst was used as working electrode (Fig. 2a and Fig. S15). For comparison, control samples of NCA (P-free) and P@CA (N-free) were synthesized (Figs. S16–S17). The gaseous and liquid products from CO_2RR were measured by on-line gas chromatography and ^{1}H nuclear magnetic resonance spectroscopy (NMR), and the results showed no liquid products formed (Fig. S18). Linear sweep voltammetry (LSV) curve of P@NCA aerogel showed a much higher total current density than that of control P@CA and NCA in 1.0 M $KHCO_3$ electrolyte (Fig. 2b). The CO and H_2 FEs of three investigated catalysts were shown in Fig. 2c and Fig. S19. Among them, the P@NCA aerogel displayed excellent CO FEs of above 90 % from − 0.3 V to − 0.9 V, and the CO FE maintained at 85 % when a potential of − 1.0 V was conducted, much higher than the other control samples of P@CA and NCA,

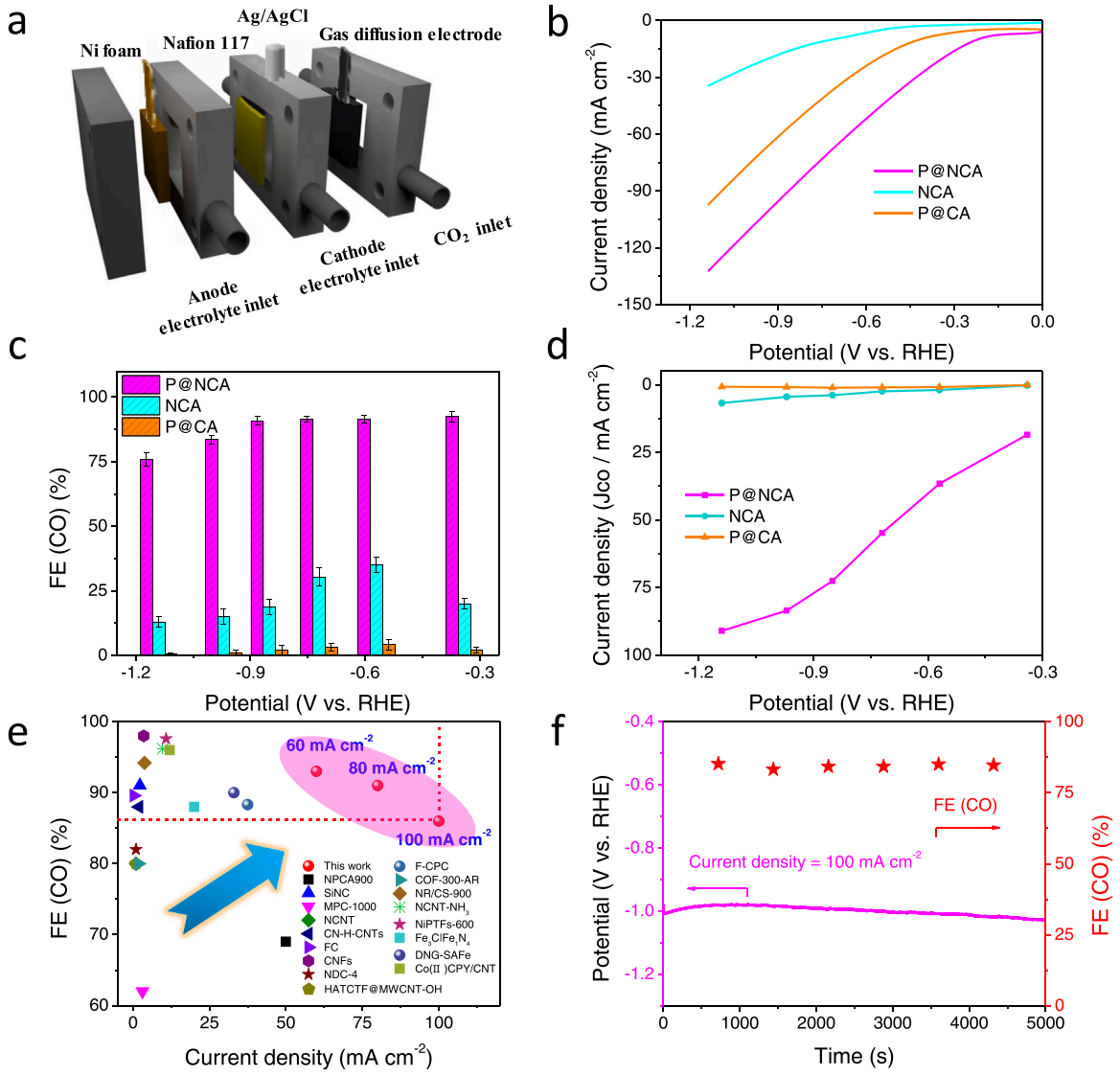

Fig. 2. (a) Assembly diagram of flow-cell reactor, (b) polarization curves of P@NCA, NCA, and P@CA, (c) CO FEs of P@NCA, NCA, and P@CA, (d) J_{CO} of P@NCA, NCA, and P@CA at different potentials, (e) CO_2RR activity comparison of P@NCA with other reported metal-free or metal-N carbon catalysts, (f) stability test of P@NCA at 100 mA cm^{-2}.

indicating its superior activity in CO_2RR [37]. In addition, the partial current densities of CO (J_{CO}) for the three catalysts were calculated. As shown in Fig. 2d, the P@NCA aerogel showed a much higher J_{CO} of 90 mA cm^{-2} than the NCA (10 mA cm^{-2}) and P@CA (1.2 mA cm^{-2}) at an applied potential of − 1.2 V, revealing the synergistic roles of N and P species in the P@NCA aerogel to boost the CO_2RR activity enhancement. Compared with other previously reported state-of-the-art CO_2RR catalysts from metal-free to metal-N carbon materials (Fig. 2e), the as-prepared P@NCA aerogel showed a top-of-the-range CO_2RR performance in terms of CO FE and current density. Moreover, the catalytic stability of P@NCA aerogel at an industrial-level current density of 100 mA cm^{-2} for CO_2RR was tested, and no obvious decay in CO FE was observed during 5000 s continuous reaction (Fig. 2f and Fig. S20), suggesting a superb durability [38,39].

In order to explore the influence of pyrolysis temperature on the performance trend of CO_2RR, control samples of P@NCA aerogels carbonized at different temperatures of 800, 900, and 1100 °C were prepared, denoted as P@NCA-800, P@NCA-900, and P@NCA-1100 [40]. And the corresponding electrochemical CO_2RR tests were performed in H-type cell (Figs. S21–S26). Clearly, a peak-like trend of CO_2RR activity from top to bottom with the change of temperature was observed. Especially, the P@NCA aerogel (Fig. 3a) showed a much higher maximum CO FE of 94 % than the P@NCA-1100 (86 %), P@NCA-900 (76 %), and P@NCA-800 (13 %) at − 0.7 V. The same peak-like trend of CO_2RR activity can also be observed for J_{CO} in Fig. 3b, in which the P@NCA aerogel delivered a high J_{CO} of 5.2 mA cm^{-2} at − 0.9 V, which was much higher than the P@NCA-1100 (4.2 mA cm^{-2}), P@NCA-900 (1.7 mA cm^{-2}), and P@NCA-800 (0.1 mA cm^{-2}) at the same potential, respectively. Tafel slope of P@NCA aerogel was calculated as 92.1 mV dec^{-1} (Fig. 3c), which was lower than that of P@NCA-1100 (98.5 mV dec^{-1}), P@NCA-900 (238.5 mV dec^{-1}), and P@NCA-800 (390.2 mV dec^{-1}), indicating a rapid CO_2 reaction kinetics on P@NCA aerogel. It is worth noting that the value of 92.1 mV dec^{-1} is close to the theoretical value of CO_2 protonation step, indicating that the rate determining step of CO_2RR over P@NCA aerogel is the process of CO_2 into *COOH intermediate [41]. Moreover, among all of the investigated samples, the P@NCA aerogel delivered the lowest electron transport resistance (Fig. S27), revealing its good electron transfer capability in CO_2RR process [42]. Further, the P@NCA aerogel showed a higher capacitance of double layer (C_{dl}) value of 29.1 mF cm^{-2} than the P@NCA-900 (24.8 mF cm^{-2}), P@NCA-1100 (19.3 mF cm^{-2}), and P@NCA-800 (1.7 mF cm^{-2}), respectively, suggesting its largest

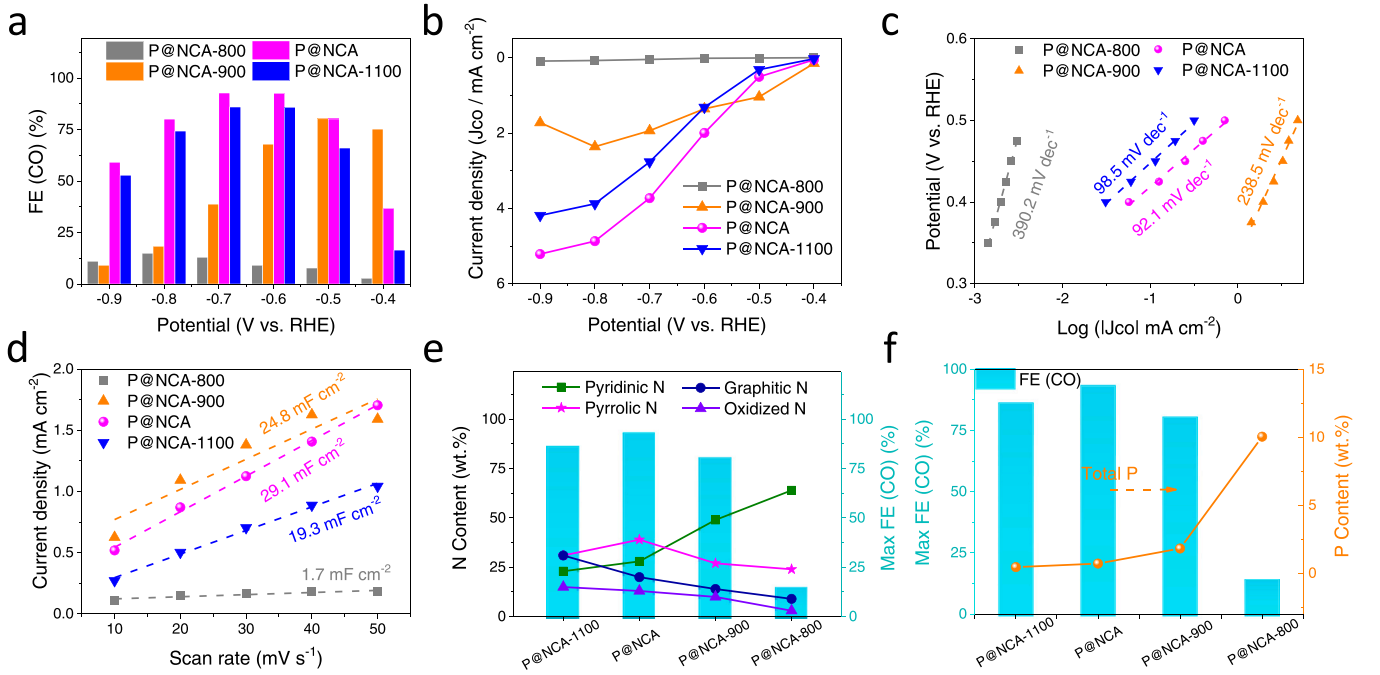

Fig. 3. (a) CO FEs and (b) corresponding J_{CO} of P@NCA-800, P@NCA-900, P@NCA, and P@NCA-1100 at different potentials in H-type cell, (c) Tafel slopes and (d) calculated C_{dl} values of P@NCA-800, P@NCA-900, P@NCA, and P@NCA-1100, (e) CO FEs and contents of fitted N species for P@NCA-800, P@NCA-900, P@NCA, and P@NCA-1100, (f) CO FEs and content of P species for P@NCA-800, P@NCA-900, P@NCA, and P@NCA-1100.

electrochemically active surface area in CO_2RR (Fig. 3d and Fig. S28) [43].

For further determining the actual active sites of P@NCA aerogel in CO_2RR, the relationship between N, P contents and CO FEs was analyzed for P@NCA and P@NCA-800/900/1100 samples. In Fig. 3e and Fig. S29, four different types of N species were fitted by high-resolution N 1s XPS spectra, and we observed that only the content of pyrrolic-N was consistent well with the change trend of CO FE, indicating that the pyrrolic-N was involved in CO_2RR as the real active sites. In contrast, the content of P species was uncorrelated with the changing trend of CO FE (Fig. 3f), revealing that the P species was not acted as main active sites that contributed to the adsorption and transformation reaction of CO_2 molecules. Based on this point, it is speculated that the P species possibly acted as a cocatalytic atom to accelerate the CO_2RR kinetics via changing the electronic structure of pyrrolic-N [44].

In order to deeply discover the intrinsic promoting effect of doped P atoms on P@NCA aerogel for CO_2RR, in-situ ATR-FTIR tests were performed from − 0.3 V to − 1.2 V (Fig. S30). As shown in Fig. 4a-b, three positive peaks located at 1395, 1420, and 1670 cm^{-1} are assigned to the CO_3^{2-}, *COOH and H_2O, respectively, indicating the generation of adsorbed *COOH intermediates. At the same time, two negative peaks located at 2360 and 1960 cm^{-1} are classified as CO_2 and *CO respectively, demonstrating that both of them are gradually consumed during CO_2RR process [45]. Among them, the *COOH intermediate is continuously generated from − 0.8 V to − 1.2 V, while the CO_2 is gradually consumed, suggesting that the protonation process from CO_2 to *COOH intermediate is rate-determining step. To further investigate the source of protons during protonation step of CO_2, the J_{CO} of P@NCA aerogel were tested in different concentrations of $KHCO_3$ (Fig. S31). In Fig. 4c, the slope value was calculated to be 0.2 according to the linear relationship between the concentration of $KHCO_3$ electrolyte and J_{CO}, which revealed a zero-order dependence between CO_2RR rate with $KHCO_3$ concentration. This result confirmed that the proton is mainly derived from water when the protonation step is performed in CO_2RR [46]. As a comparison, the intensity of positive characteristic peak representing the accumulated water molecules at 1670 cm^{-1} in control NCA was much higher than that in P@NCA (Fig. 4d-e), indicating the significantly accelerated water dissociation process in P@NCA with introducing P species. Notably, the *CO intermediates (1960 cm^{-1}) adsorbed on P@NCA aerogel and NCA are continuously consumed and accumulated, respectively, suggesting the P@NCA aerogel possess an accelerated *CO desorption step compared with NCA in CO_2RR. To further confirm the accelerating effect of P@NCA aerogel on water dissociation with the incorporation of P, the kinetic isotope effect (KIE) were investigated. In Fig. 4f, the KIE value of P@NCA aerogel was calculated to be 1.1, which is lower than that of NCA (1.5), revealing the processes of water dissociation and subsequent proton transfer are promoted with the assistance of P species [47]. Meanwhile, according to the Arrhenius equation, the activation energies of P@NCA aerogel and NCA are calculated to be 10.33 and 32.50 KJ mol^{-1}, respectively (Fig. 4g and Fig. S32) [48,49], indicating a reduced energy required for CO_2-CO conversion under the synergistic effect of N and P species. Based on the above analysis, the corresponding CO_2RR mechanism is proposed (Fig. 4h and Fig. S33): under the assistance of P atoms, the dissociation of water molecules is obviously accelerated on P@NCA aerogel, which results in a rapid protonation process of CO_2 to *COOH. Subsequently, in the final CO desorption step, the doped P atoms promotes the more quickly desorption of *CO intermediate from real active sites of pyrrolic-N, thus boosting the whole CO_2RR activity of P@NCA aerogel.

In order to reveal the intrinsic mechanism of P@NCA aerogel in CO_2RR, three different types of N, P co-doped graphene constructions were studied by first principles calculation, including graphitic N-P, pyridinic N-P and pyrrolic N-P (Fig. 5a), and the calculation details were given in Supporting Information. Due to the radius of P atom is larger than N and C atoms, the plane of graphene is wrinkled with P atom protruding out. To clarify the reaction thermodynamic behavior, the CO_2-to-CO conversion is evaluated by calculating the Gibbs free energies as following elementary steps

$$* + CO_2 + H^+ + e^- \rightarrow *COOH$$

$$*COOH + H^+ + e^- \rightarrow * CO + H_2O$$

$$*CO \rightarrow * + CO$$

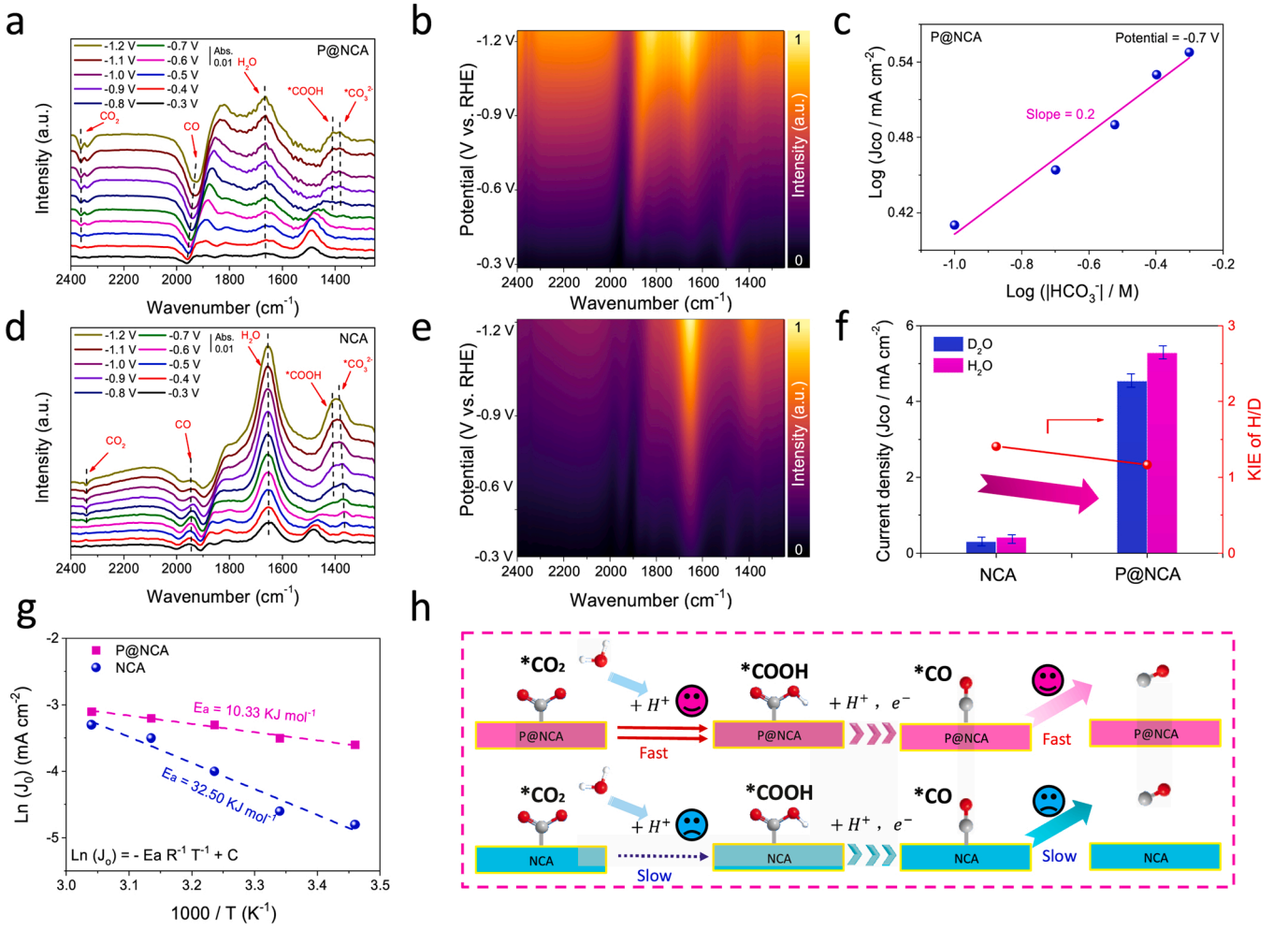

Fig. 4. (a-b) In situ ATR-FTIR spectra and corresponding contour image of P@NCA tested from − 0.3 V to − 1.2 V, (c) J_{CO} of P@NCA at different $KHCO_3$ concentrations, (d-e) in situ ATR-FTIR spectra and corresponding contour image of NCA tested from − 0.3 V to − 1.2 V, (f) J_{CO} and KIE values of H/D for NCA and P@NCA, (g) the activation energies for P@NCA and NCA in CO_2RR, (h) mechanism diagram of CO_2RR for P@NCA and NCA.

As shown in Fig. 5b, the maximum reaction energy steps are the formation of *COOH intermediate for graphene doped with graphitic N-P (2.59 eV), pyridinic N-P (1.24 eV), and pyrrolic N-P (0.22 eV). As a result, the pyrrolic-N of graphene doped with pyrrolic N-P presents an excellent activity for CO_2RR. It is noting that, the pyrrolic-N without P doping exhibits the much stronger adsorption for *COOH and *CO intermediates than the pyrrolic N-P, which induces to the large reaction energy ($\Delta G = 0.81$ eV) of CO desorption step for NCA. In addition, the thermodynamics of competitive HER is evaluated in Fig. 5c. The calculation results show that the *H adsorption strength on pyrrolic-N of graphene is too strong, which leads to the inhibition of the adsorption of *COOH and *CO intermediates. With P doping nearby, the strength of *H adsorption on pyrrolic-N is decreased markedly, contributing the formation of *COOH intermediate and CO selectivity of CO_2RR. To uncover the effect of P doping in reactivity, charge density difference is further analyzed between pyrrolic-N with and without P surrounding. It is clearly seen that the doping of P atom efficiently induces the increase of charge density for pyrrolic-N (Fig. 5d). Moreover, the electronic structure of pyrrolic-N is modified by P doping shown in Fig. 5e. The orbital wave function (squared) close to the Fermi level (Fig. 5f) shows that the pyrrolic-N site of NCA has dominantly occupied orbital contribution with perpendicular orientation to the layer, which is favorable to strong electronic coupling with maximum orbital overlap and consequently strong intermediates adsorption [50]. With P doping, the orientation of orbital wave function close to the Fermi level incline, inducing the reduction of components outside the vertical plane. As a result, the hybridization between the molecular orbital of *CO intermediate and the p orbital of N atom is weakened. Therefore, the decreased adsorption strength for CO on pyrrolic N-P favors the last elementary reaction step, i.e., *CO desorption.

Inspired by the outstanding CO_2RR performance of P@NCA aerogel, an aqueous Zn-CO_2 battery with P@NCA aerogel cathode and Zn plate anode was assembled to evaluate the practical application ability of CO_2RR (Fig. 6a). The 6.0 M KOH containing 0.2 M $Zn(CH_3COO)_2$ and CO_2-saturated 0.5 M $KHCO_3$ solutions were used as anolyte and catholyte, respectively [51]. In Fig. 6b, the discharge voltage curve showed an open-circuit voltage of 0.8 V and a high power density of 0.8 mW cm^{-2} for P@NCA aerogel. In addition, the P@NCA aerogel presented a maximum CO FE of 92 % at the discharge current density of 2.0 mA cm^{-2} (Fig. 6c), demonstrating the superior CO_2RR activity in Zn-CO_2 battery. Based on the good power density of P@NCA aerogel, two Zn-CO_2 batteries connecting in series can light up a red light-emitting diode in Fig. 6d, suggesting a large potential of P@NCA aerogel for energy conversion. Meanwhile, the galvanostatic charge-discharge cycling test of P@NCA aerogel was further performed at 0.5 mA cm^{-2}, in which no obviously enlarged voltage gap was observed within 20 h (Fig. 6e), demonstrating the excellent durability.

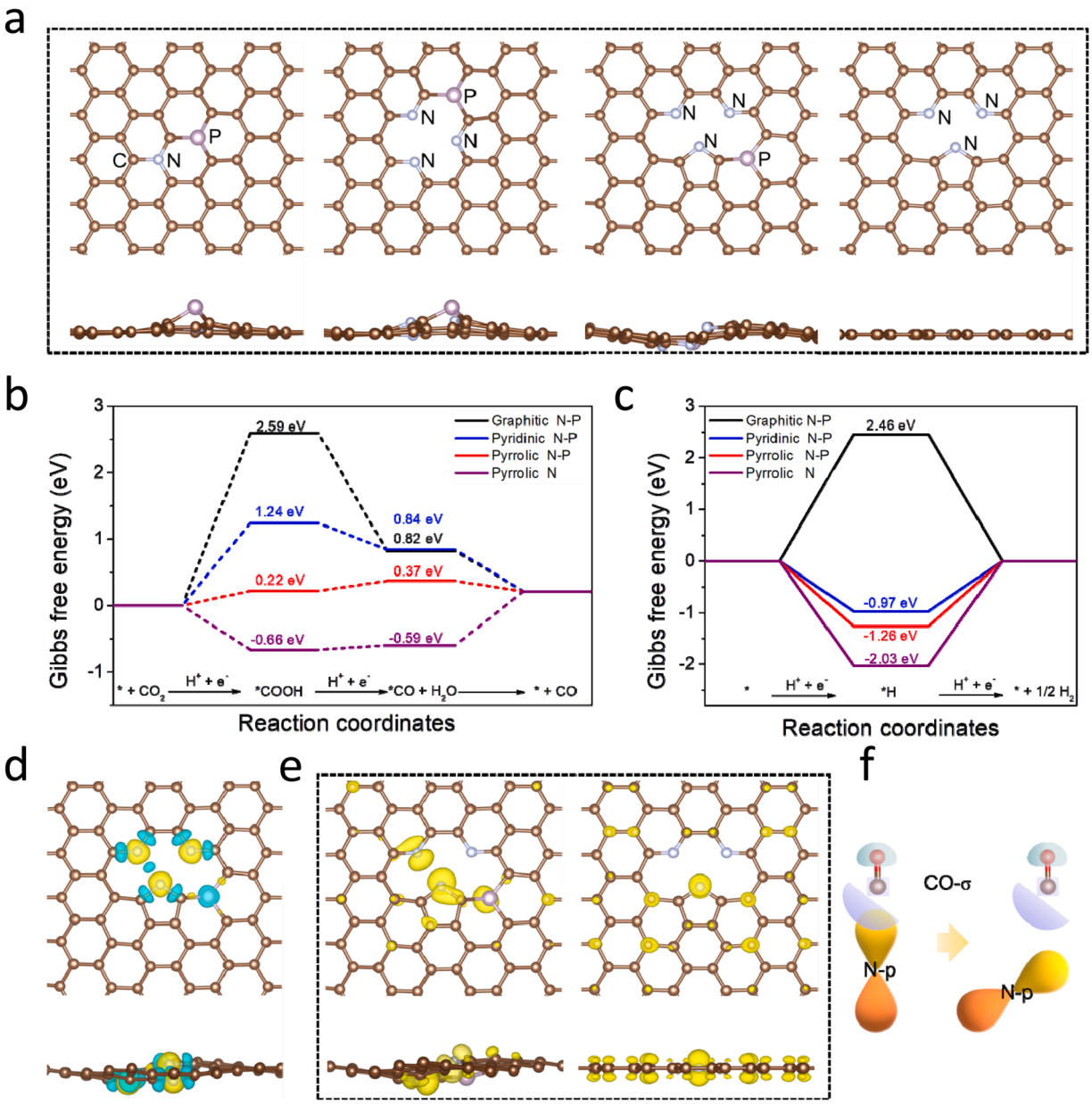

Fig. 5. (a) The constructions of graphene with graphitic N-P, pyridinic N-P, pyrrolic N-P and pyrrolic N. The Gibbs free energy profiles of (b) CO_2-CO and (c) HER reaction. (d) The charge density differences between pyrrolic N-P and pyrrolic N, iso-value 0.03 |e| $Å^{-3}$. (e) The occupied orbital distribution near Fermi-level for graphene doped with pyrrolic N-P and pyrrolic N. (f) The schematic diagram for orbital interaction with different orientation.

4. Conclusions

In summary, we have developed a new type of metal-free P@NCA aerogel catalyst with uniformly dispersed P, N sites and 3D mesh-like structure, that demonstrates highly efficient CO_2RR performance. A wide potential window from − 0.3 V to − 0.9 V with CO FE of above 90 % was achieved on P@NCA aerogel, which exceeded the most of the previously reported metal-free carbon based CO_2RR catalysts. More importantly, the P@NCA aerogel delivered a superb CO_2RR activity with a high CO FE of 85 % under 100 mA cm^{-2}. Experimental observations and in situ ATR-FTIR results confirmed the real active site of pyrrolic-N species on P@NCA aerogel, while the P atoms anchored around the pyrrolic-N site played a dominant role in accelerating water dissociation to boost the proton transfer rate, thus promoting the formation of key *COOH intermediate. Further theoretical simulation results are in good agreement with our experiments, which allows us to identify the reaction mechanism for how P doping affects CO_2RR activity and selectivity. Furthermore, a rechargeable Zn-CO_2 battery with P@NCA aerogel cathode realized a maximum power density of 0.8 mW cm^{-2}. The accelerating proton feeding via P doping method reported in this work opens up a horizon for designing the highly efficient metal-free carbon based catalyst useful for CO_2RR and other electrochemical reactions, including N_2 reduction, O_2 reduction, and water electrolysis.

CRediT authorship contribution statement

Wanzhen Zheng: Conceptualization, Methodology, Investigation, Writing – original draft, Writing – review & editing. **Dashuai Wang:** Conceptualization, Investigation, Software. **YiKai Zhang:** Methodology, Investigation, Writing – review & editing. **Sixing Zheng**: Investigation. **Bin Yang:** Investigation. **Zhongjian Li:** Investigation. **Raul D. Rodriguez:** Investigation. **Tao Zhang:** Investigation. **Lecheng Lei:** Investigation, Funding acquisition. **Siyu Yao:** Supervision. **Yang Hou:** Conceptualization, Writing – review & editing, Resources, Supervision,

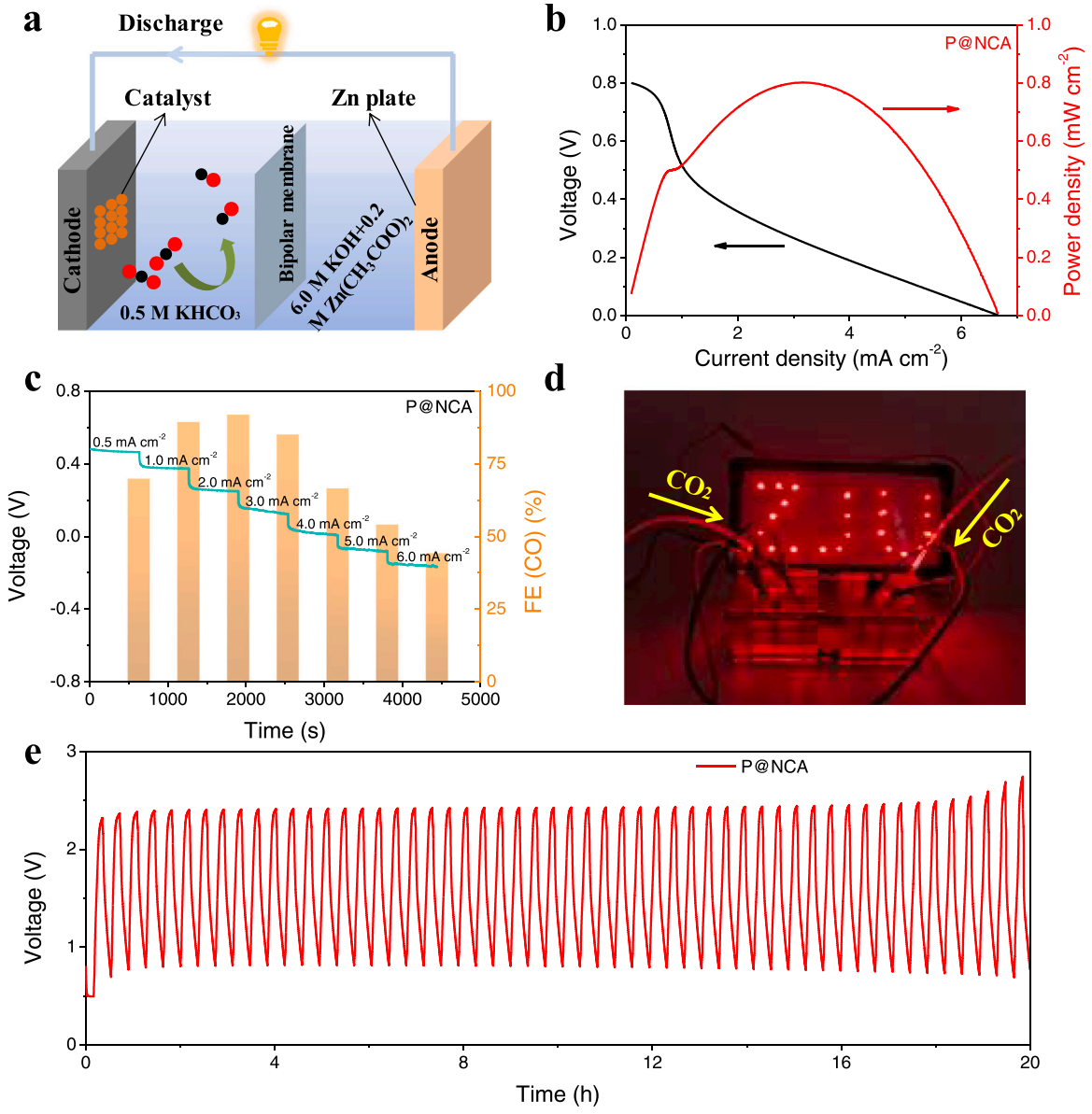

Fig. 6. (a) Schematic configuration of Zn-CO_2 battery, (b) discharge curve and power density of P@NCA, (c) CO FE and current density of P@NCA in Zn-CO_2 battery, (d) digital photo of light-driven by two Zn-CO_2 batteries, (e) galvanostatic charge-discharge cycling curve of P@NCA at 0.5 mA cm^{-2}.

Funding acquisition.

Declaration of Competing Interest

The authors declare that they have no known competing financial interests or personal relationships that could have appeared to influence the work reported in this paper.

Data Availability

Data will be made available on request.

Acknowledgements

The authors greatly acknowledge the financial support from the Fundamental Research Funds for the Central Universities (226-2022-00044 and 226-2022-00055), the National Natural Science Foundation of China (U22A20432, 22211530045, 22278364, 21922811, 22178308, 21878270), the Zhejiang Provincial Natural Science Foundation of China (LR19B060002), Zhejiang University Global Partnership Fund, the Startup Foundation for Hundred-Talent Program of Zhejiang University.

Appendix A. Supporting information

Supplementary data associated with this article can be found in the online version at doi:10.1016/j.nanoen.2022.107980.

References

[1] G. Wang, J. Chen, Y. Ding, P. Cai, L. Yi, Y. Li, C. Tu, Y. Hou, Z. Wen, L. Dai, Chem. Soc. Rev. 50 (2021) 4993–5061.
[2] T. Wang, Q. Zhao, Y. Fu, C. Lei, B. Yang, Z. Li, L. Lei, G. Wu, Y. Hou, Small Methods 3 (2019), 1900210.
[3] C. Kim, J.C. Bui, X. Luo, J.K. Cooper, A. Kusoglu, A.Z. Weber, A.T. Bell, Nat. Energy 6 (2021) 1026–1034.
[4] X. Wang, Q. Zhao, B. Yang, Z. Li, Z. Bo, K.H. Lam, N.M. Adli, L. Lei, Z. Wen, G. Wu, Y. Hou, J. Mater. Chem. A 7 (2019) 25191–25202.
[5] H. Wu, J. Li, K. Qi, Y. Zhang, E. Petit, W. Wang, V. Flaud, N. Onofrio, B. Rebiere, L. Huang, C. Salameh, L. Lajaunie, P. Miele, D. Voiry, Nat. Commun. 12 (2021) 7210.

[6] Z. Chen, X. Zhang, W. Liu, M. Jiao, K. Mou, X. Zhang, L. Liu, Energy Environ. Sci. 14 (2021) 2349–2356.
[7] Z. Zeng, L.Y. Gan, H. Bin Yang, X. Su, J. Gao, W. Liu, H. Matsumoto, J. Gong, J. Zhang, W. Cai, Z. Zhang, Y. Yan, B. Liu, P. Chen, Nat. Commun. 12 (2021) 4088.
[8] C. Chen, X. Sun, X. Yan, Y. Wu, H. Liu, Q. Zhu, B.B.A. Bediako, B. Han, Angew. Chem. Int. Ed. 59 (2020) 11123–11129.
[9] B. Zhang, J. Zhang, F. Zhang, L. Zheng, G. Mo, B. Han, G. Yang, Adv. Funct. Mater. 30 (2020), 1906194.
[10] Z. Fang, P. Li, G. Yu, Adv. Mater. 32 (2020), 2003191.
[11] J. Xie, X. Zhao, M. Wu, Q. Li, Y. Wang, J. Yao, Angew. Chem. Int. Ed. 57 (2018) 9640–9644.
[12] X. Cui, Z. Pan, L. Zhang, H. Peng, G. Zheng, Adv. Energy Mater. 7 (2017), 1701456.
[13] X. Duan, J. Xu, Z. Wei, J. Ma, S. Guo, S. Wang, H. Liu, S. Dou, Adv. Mater. 29 (2017), 1701784.
[14] H. Yang, Y. Wu, Q. Lin, L. Fan, X. Chai, Q. Zhang, J. Liu, C. He, Z. Lin, Angew. Chem. Int. Ed. 57 (2018) 15476–15480.
[15] Y. Zhu, K. Lv, X. Wang, H. Yang, G. Xiao, Y. Zhu, J. Mater. Chem. A 7 (2019) 14895–14903.
[16] N. Wanninayake, Q. Ai, R. Zhou, M.A. Hoque, S. Herrell, M.I. Guzman, C. Risko, D. Y. Kim, Carbon 157 (2020) 408–419.
[17] W. Ni, Y. Xue, X. Zang, C. Li, H. Wang, Z. Yang, Y.-M. Yan, ACS Nano 14 (2020) 2014–2023.
[18] F. Pan, A. Liang, Y. Duan, Q. Liu, J. Zhang, Y. Li, J. Mater. Chem. A 5 (2017) 13104–13111.
[19] M.A. Ghausi, J. Xie, Q. Li, X. Wang, R. Yang, M. Wu, Y. Wang, L. Dai, Angew. Chem. Int. Ed. 57 (2018) 13135–13139.
[20] A. Laemont, S. Abednatanzi, P.G. Derakshandeh, F. Verbruggen, E. Fiset, Q. Qin, K. Van Daele, M. Meledina, J. Schmidt, M. Oschatz, P. Van Der Voort, K. Rabaey, M. Antonietti, T. Breugelmans, K. Leus, Green Chem. 22 (2020) 3095–3103.
[21] J. Zhang, Z. Zhao, Z. Xia, L. Dai, Nat. Nanotechnol. 10 (2015) 444–452.
[22] L. Pan, G. Yu, D. Zhai, R. Lee Hye, W. Zhao, N. Liu, H. Wang, C.K. Tee Benjamin, Y. Shi, Y. Cui, Z. Bao, Proc. Natl. Acad. Sci. USA 109 (2012) 9287–9292.
[23] P. Li, Z. Jin, Y. Qian, Z. Fang, D. Xiao, G. Yu, ACS Energy Lett. 4 (2019) 1793–1802.
[24] W. Ni, Z. Liu, Y. Zhang, C. Ma, H. Deng, S. Zhang, S. Wang, Adv. Mater. 33 (2021), 2003238.
[25] Y. Kong, Y. Li, X. Sang, B. Yang, Z. Li, S. Zheng, Q. Zhang, S. Yao, X. Yang, L. Lei, S. Zhou, G. Wu, Y. Hou, Adv. Mater. 34 (2022), 2103548.
[26] S. Feng, W. Zheng, J. Zhu, Z. Li, B. Yang, Z. Wen, J. Lu, L. Lei, S. Wang, Y. Hou, Appl. Catal. B 270 (2020), 118908.
[27] Y. Zhang, X. Wang, S. Zheng, B. Yang, Z. Li, J. Lu, Q. Zhang, N.M. Adli, L. Lei, G. Wu, Y. Hou, Adv. Funct. Mater. 31 (2021), 2104377.
[28] W. Zheng, Y. Wang, L. Shuai, X. Wang, F. He, C. Lei, Z. Li, B. Yang, L. Lei, C. Yuan, M. Qiu, Y. Hou, X. Feng, Adv. Funct. Mater. 31 (2021), 2008146.
[29] W. Zheng, J. Yang, H. Chen, Y. Hou, Q. Wang, M. Gu, F. He, Y. Xia, Z. Xia, Z. Li, B. Yang, L. Lei, C. Yuan, Q. He, M. Qiu, X. Feng, Adv. Funct. Mater. 30 (2020), 1907658.
[30] T. Wang, X. Sang, W. Zheng, B. Yang, S. Yao, C. Lei, Z. Li, Q. He, J. Lu, L. Lei, L. Dai, Y. Hou, Adv. Mater. 32 (2020), 2002430.
[31] J. Chen, Z. Li, X. Wang, X. Sang, S. Zheng, S. Liu, B. Yang, Q. Zhang, L. Lei, L. Dai, Y. Hou, Angew. Chem. Int. Ed. 61 (2022), e202111683.
[32] K. Li, S. Zhang, X. Zhang, S. Liu, H. Jiang, T. Jiang, C. Shen, Y. Yu, W. Chen, Nano Lett. 22 (2022) 1557–1565.
[33] L. Li, Y. Zhang, H. Lu, Y. Wang, J. Xu, J. Zhu, C. Zhang, T. Liu, Nat. Commun. 11 (2020) 62.
[34] Z. Li, A. Cao, Q. Zheng, Y. Fu, T. Wang, K.T. Arul, J.-L. Chen, B. Yang, N.M. Adli, L. Lei, C.-L. Dong, J. Xiao, G. Wu, Y. Hou, Adv. Mater. 33 (2021), 2005113.
[35] Z. Li, Q. Zeng, Z. Ye, W. Zheng, X. Sang, C.-L. Dong, B. Yang, S. Pardiwala, J. Lu, L. Lei, G. Wu, Y. Hou, Nano Energy 87 (2021), 106187.
[36] X. Wang, S. Feng, W. Lu, Y. Zhao, S. Zheng, W. Zheng, X. Sang, L. Zheng, Y. Xie, Z. Li, B. Yang, L. Lei, S. Wang, Y. Hou, Adv. Funct. Mater. 31 (2021), 2104243.
[37] Y. Guo, Y. Wang, Y. Shen, Z. Cai, Z. Li, J. Liu, J. Chen, C. Xiao, H. Liu, W. Lin, C. Wang, J. Am. Chem. Soc. 142 (2020) 21493–21501.
[38] S. Li, S. Zhao, X. Lu, M. Ceccato, X.-M. Hu, A. Roldan, J. Catalano, M. Liu, T. Skrydstrup, K. Daasbjerg, Angew. Chem. Int. Ed. 60 (2021) 22826–22832.
[39] J. Pei, T. Wang, R. Sui, X. Zhang, D. Zhou, F. Qin, X. Zhao, Q. Liu, W. Yan, J. Dong, L. Zheng, A. Li, J. Mao, W. Zhu, W. Chen, Z. Zhuang, Energy Environ. Sci. 14 (2021) 3019–3028.
[40] X. Wang, Y. Wang, X. Sang, W. Zheng, S. Zhang, L. Shuai, B. Yang, Z. Li, J. Chen, L. Lei, N.M. Adli, M.K.H. Leung, M. Qiu, G. Wu, Y. Hou, Angew. Chem. Int. Ed. 60 (2021) 4192–4198.
[41] Y. Chen, C.W. Li, M.W. Kanan, J. Am. Chem. Soc. 134 (2012) 19969–19972.
[42] Z.-H. Zhu, B.-H. Zhao, S.-L. Hou, X.-L. Jiang, Z.-L. Liang, B. Zhang, B. Zhao, Angew. Chem. Int. Ed. 60 (2021) 23394–23402.
[43] Y. Wang, B.J. Park, V.K. Paidi, R. Huang, Y. Lee, K.-J. Noh, K.-S. Lee, J.W. Han, ACS Energy Lett. 7 (2022) 640–649.
[44] C. Xu, A. Vasileff, D. Wang, B. Jin, Y. Zheng, S. Qiao, Nanoscale Horiz. 4 (2019) 1411–1415.
[45] T. Jiang, Y. Zhou, X. Ma, X. Qin, H. Li, C. Ding, B. Jiang, K. Jiang, W. Cai, ACS Catal. 11 (2021) 840–848.
[46] J. Rosen, G.S. Hutchings, Q. Lu, S. Rivera, Y. Zhou, D.G. Vlachos, F. Jiao, ACS Catal. 5 (2015) 4293–4299.
[47] X. Wang, X. Sang, C.-L. Dong, S. Yao, L. Shuai, J. Lu, B. Yang, Z. Li, L. Lei, M. Qiu, L. Dai, Y. Hou, Angew. Chem. Int. Ed. 60 (2021) 11959–11965.
[48] H. Su, W. Zhou, W. Zhou, Y. Li, L. Zheng, H. Zhang, M. Liu, X. Zhang, X. Sun, Y. Xu, F. Hu, J. Zhang, T. Hu, Q. Liu, S. Wei, Nat. Commun. 12 (2021) 6118.
[49] X. Wang, C. Xu, M. Jaroniec, Y. Zheng, S.-Z. Qiao, Nat. Commun. 10 (2019) 4876.
[50] Y. Wu, J. Cai, Y. Xie, S. Niu, Y. Zang, S. Wu, Y. Liu, Z. Lu, Y. Fang, Y. Guan, X. Zheng, J. Zhu, X. Liu, G. Wang, Y. Qian, Adv. Mater. 32 (2020), 1904346.
[51] X. Wang, J. Xie, M.A. Ghausi, J. Lv, Y. Huang, M. Wu, Y. Wang, J. Yao, Adv. Mater. 31 (2019), 1807807.

Wanzhen Zheng is a Ph.D. candidate under the supervision of Prof. Yang Hou in Key Laboratory of Biomass Chemical Engineering of Ministry of Education, College of Chemical and Biological Engineering, Zhejiang University. Her research interest is to design non-noble metal/carbon based electrocatalysts for CO_2 electroreduction.

Dashuai Wang received his Ph.D. degree from Jilin university in 2019, and then did 3 years of postdoctoral research in Shenzhen Geim Graphene Center, Tsinghua-Berkeley Shenzhen Institute & Tsinghua Shenzhen International Graduate School, Tsinghua University. He has been a Professor in Institute of Zhejiang University – Quzhou since 2021. His current research focuses on first principles theoretical calculations.

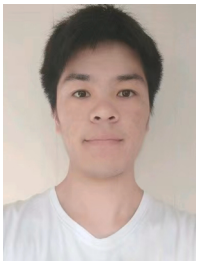

Yikai Zhang is a graduate student under the supervision of Prof. Yang Hou in Key Laboratory of Biomass Chemical Engineering of Ministry of Education, College of Chemical and Biological Engineering, Zhejiang University. His research interest is to design carbon based electrocatalysts for CO_2 electroreduction.

Sixing Zheng is a Ph.D. candidate under the supervision of Prof. Yang Hou in Key Laboratory of Biomass Chemical Engineering of Ministry of Education, College of Chemical and Biological Engineering, Zhejiang University. His research interest is to design transition metal/carbon based electrocatalysts for CO_2 electroreduction.

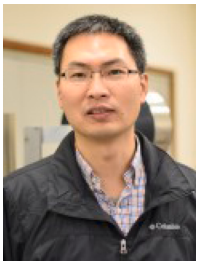

Prof. Bin Yang is an Associate Professor in the College of Chemical Engineering at Zhejiang University. He graduated from Zhejiang University in 2001 and 2004, with his Bachelor's degree and Master's degree in Environmental Engineering. In 2012, he received his Ph.D. degree from the HKUST. His research fields focus on the advanced oxidation process for wastewater treatment, membrane fouling control, and novel materials for energy conversions.

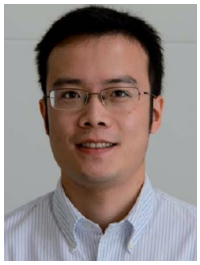

Prof. Zhongjian Li is an Associate Professor in the College of Chemical and Biological Engineering at Zhejiang University. He received his Ph.D. degree from the Department of Environmental Engineering of Zhejiang University. His recent researches focus on converting CO_2 into fuels based on bio-inorganic hybrid catalysts system and developing wastewater treatment processes using bioelectrochemical systems.

Prof. Lecheng Lei is a Professor at the College of Chemical and Biological Engineering at Zhejiang University. He obtained his Ph.D. degree from Zhejiang University and the HKUST, and then did postdoctoral research in the School of Chemical Engineering at Karlsruhe University in Germany. His research fields focus on the new water treatment technology, chemical safety, and industrial ecology.

Prof. Raul D. Rodriguez received a Ph.D. in Physics and Chemistry of Nanomaterials in 2009. He was appointed in 2017 as a Full Professor at Tomsk Polytechnic University, Tomsk, Russia. He focuses on flexible electronics, particularly novel plasmonic and 2D nanomaterials for technological developments, including biomedicine, optoelectronics, energy, and safety applications.

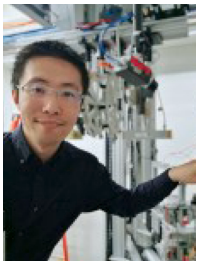

Prof. Siyu Yao is a Professor at the College of Chemical and Biological Engineering at Zhejiang University. He received his Ph.D. degree from the Peking University in 2014, and then did postdoctoral research at Brookhaven National Laboratory, USA. His current researches mainly focus on exploring the heterogeneous catalytic processes of small molecules activation and conversion into high value-added chemicals.

Prof. Tao Zhang has studied and worked in Sichuan University, Dresden University of Technology, Cavendish Laboratory of Cambridge University, and Dresden Advanced Electronic Devices Research Center (cfaed). He is currently a professor at the Ningbo Institute of Materials Technology and Engineering, CAS, the head of the interface functional polymer materials team. He commits to the design and synthesis of new materials of two-dimensional conjugated polymers and the basic research on the application of marine functional materials.

Prof. Yang Hou is a Professor at the College of Chemical and Biological Engineering at Zhejiang University. He received his Ph.D. degree from the School of Environmental Science & Technology of Dalian University of Technology in 2011, and then did postdoctoral research at the University of California, Riverside, University of Wisconsin-Milwaukee, and TU Dresden. His current researches mainly focus on the design and synthesis of low-dimensional materials for energy and environmental applications.